LIGO VIRGO KAGRA

LIGO–Virgo–KAGRA webinar

GWTC-3: Compact binary coalescences observed during the second part of the third observing run

6 December 2021

Webinar streaming live from **15:00 UTC**

Image credit: LIGO/Caltech/MIT/Sonoma State/Aurore Simonnet

GWTC-3: Compact Binary Coalescences Observed by LIGO and Virgo During the Second Part of the Third Observing Run

arXiv:2111.03606 • www.gw-openscience.org/GWTC-3/

15:00 UTC • 6 December 2021 • dcc.ligo.org/G2102416/public

The gravitational-wave story

1916 Einstein predicts gravitational waves in general relativity

1974 First indirect evidence of gravitational waves from binary pulsars

2015 First observation of gravitational waves at the start of O1

Observing runs
O1: 2015–2016
O2: 2016–2017
O3: 2019–2020
O4: ~2022–2023

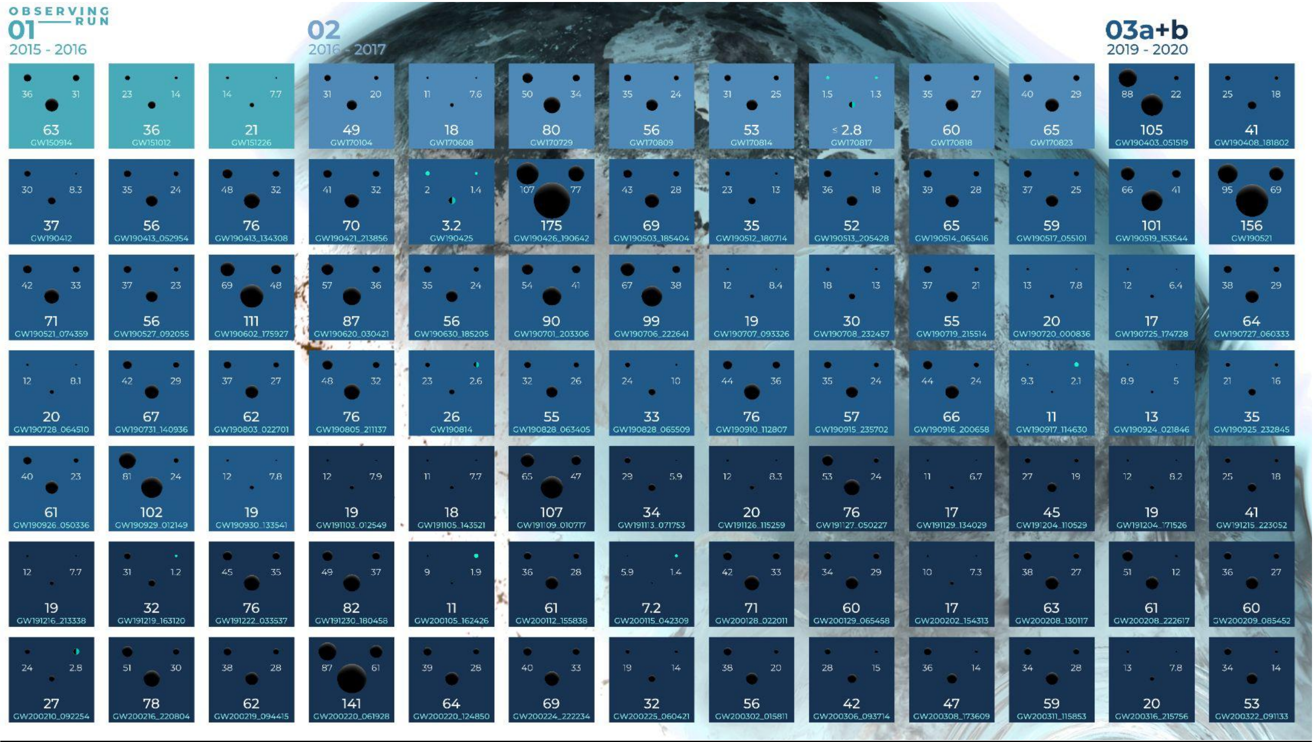

GWTC-3 webinars

Today: Compact binary coalescences observed by LIGO and Virgo during the second part of the third observing run

9 December 2021: Constraints on the cosmic expansion history from GWTC-3

10 December 2021: The population of merging compact binaries inferred using gravitational waves through GWTC-3

20 January 2022: Tests of general relativity with GWTC-3

Speakers

Francesco Di Renzo U. Pisa/INFN	Instruments
Jess McIver U. British Columbia	Data
Becca Ewing The Pennsylvania State U.	Candidate search
Isobel Romero-Shaw OzGrav/Monash U.	Source properties
Christopher Berry U. Glasgow/Northwestern U.	Q&A

Panelists

Carl Blair OzGrav/U. Western Australia	Instruments: LIGO
Loïc Rolland LAPP	Calibration
Sidd Soni MIT	Data quality
Gareth Cabourn Davies U. Portsmouth	Searches: PyCBC
Frédérique Marion LAPP	Searches: MBTA
Edoardo Milotti U. Trieste/INFN	Searches: cWB
Dimitri Estevez U. Strasbourg	Probability of astrophysical origin

Panelists

Marek Szczepańczyk U. Florida	cWB/Probability of astrophysical origin
Tri Nguyen MIT	Search sensitivity
Daniel Williams SUPA/U. Glasgow	Parameter estimation
Serguei Ossokine MPI/AEI	Waveform modeling
Meg Millhouse OzGrav/U. Melbourne	BayesWave/Glitch subtraction
Rosa Poggiani U. Pisa/INFN	Follow-up
Hannah Middleton OzGrav/Swinburne/ U. Melbourne/	Data release

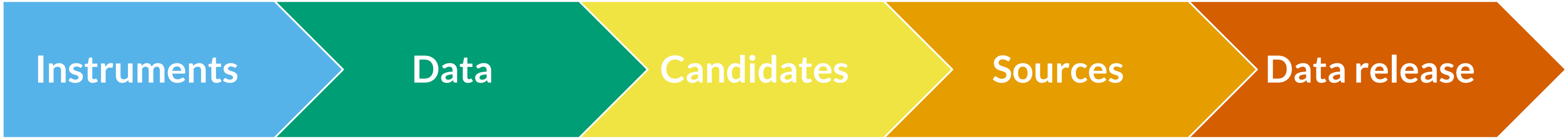
Instruments
Data
Candidates
Sources
Data release

LIGO & Virgo in O3b

Gravitational waves

Gravitational waves are ripples in spacetime caused by some of the most violent and energetic processes in the Universe

They originate from **accelerating masses**, such as the inspiral of a binary neutron star system

Effect of a plus-polarized gravitational wave on a circular array of **test masses**

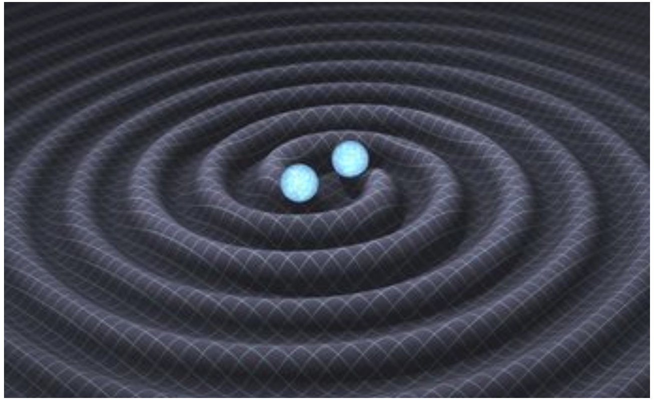

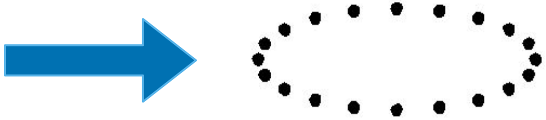

Instruments in O3b

Quantum squeezing
Vacuum state of light with phase fluctuations smaller than the normal vacuum to reduce phase noise at the expense of amplitude noise

For more on squeezing:
Tse *et al.* (2019) Phys. Rev. Lett. 123, 231107
Acernese *et al.* (2019) Phys. Rev. Lett. 123, 23110

Similar to during O3a, where the main improvements were:

- adjustment of in-vacuum squeezing for LIGO Hanford and Livingston
- increase of laser power for Virgo

After October commissioning break:

- LIGO: Adjustments to the squeezing subsystem and reduction of scattered light noise; implementation of reaction-chain tracking
- Virgo: Increased laser power; improved electronics, alignment, etalon feedback system, squeezing and software

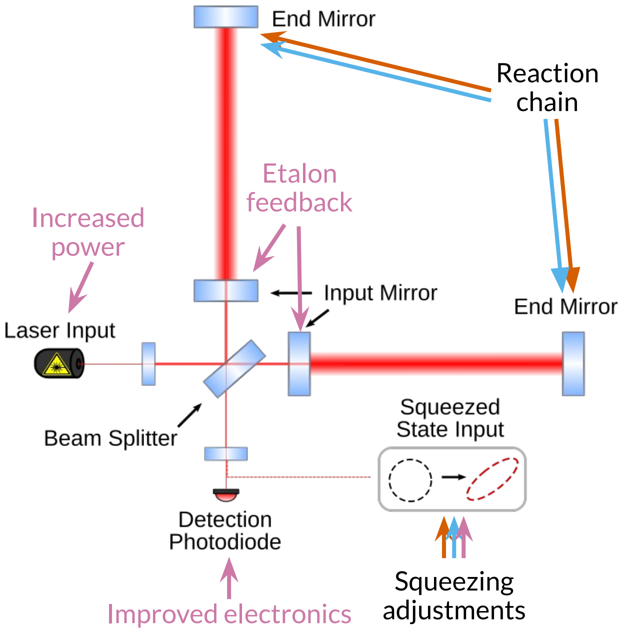

Detector sensitivity curves

Strain sensitivity can be characterized by the detector noise spectrum

A smaller value of the spectrum means lower noise at a given frequency and an increased sensitivity to signals

The previous upgrades led to a better **detector sensitivity** and also a high duty cycle, despite running through winter:

- 142.0 days with **at least one detector** observing
- 79%, 79% and 76% for Hanford, Livingston and Virgo
- Triple time 51.0%, double time 85.3% and single time 96.6%

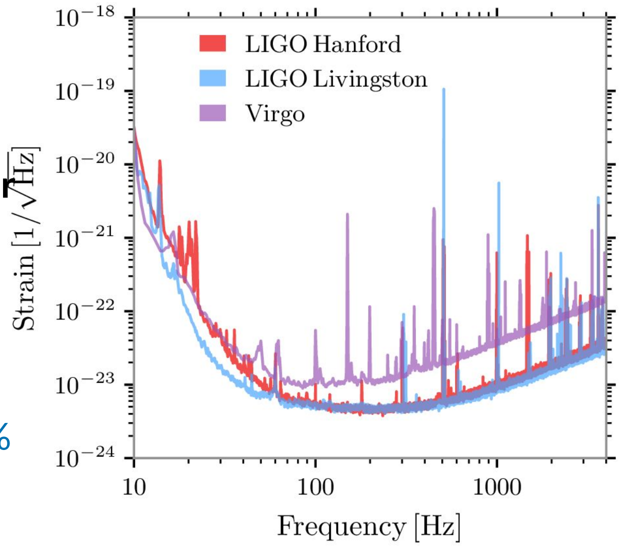

Binary neutron star ranges

The **binary neutron star (BNS) range** is a standard measure of detector sensitivity. It distance a detector is able to detect a signal from a 1.4+1.4 solar mass binary

Higher mass sources are detected at greater distances

2 Jan: squeezing improvements
28 Jan: electronics, squeezing and alignment improvements

Median BNS ranges

LIGO Hanford: 115 Mpc, LIGO Livingston: 133 Mpc, Virgo: 51 Mpc

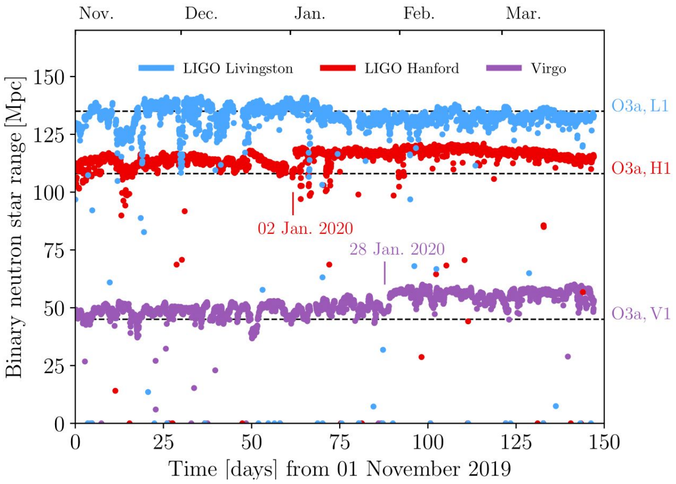

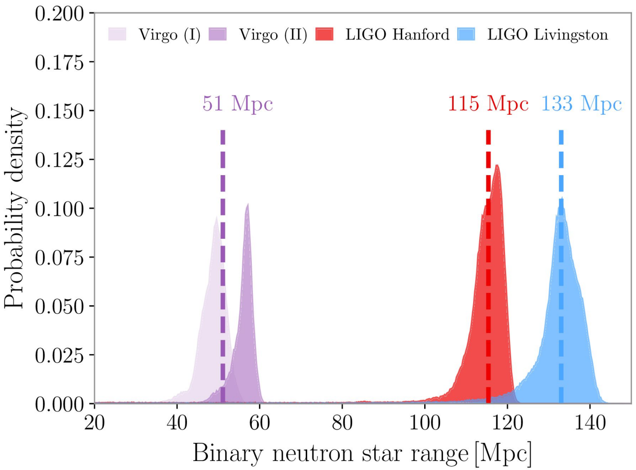


Calibration & data quality
Instruments
Data
Candidates
Sources
Data release

Calibration

Noise subtraction the same as used for GWTC-2.1

Alternate calibration versions of data for O3b are available from GWOSC

Different calibration versions apply different forms of noise subtraction

For more on calibration:
Sun *et al.* (2021) arXiv:2107.00129
Acernese *et al.* (2021) arXiv:2107.03294

Final calibrated strain data used for all results

Most sophisticated noise cleaning available used for all paper results, with one minor exception of cWB: cWB used calibrated data with all cleaning except subtraction of non-stationary coupling of power grid (as for GWTC-2)

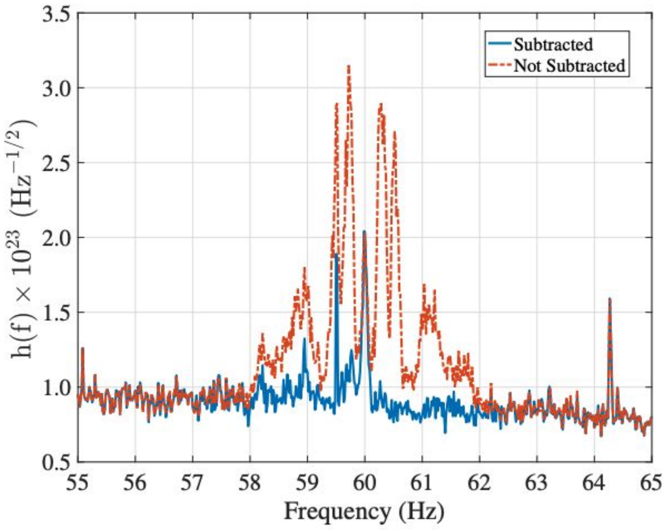

Glitch rate

Glitches are transient non-Gaussian noise. New glitch types can arise from instrument changes or sensitivity increases

A high glitch rate can drive up noise background estimates for gravitational-wave searches

For more on glitches: Davis *et al.* (2021) Class. Quant. Grav. 38, 135014

Hanford sees a significant drop in glitch rate after reaction-chain tracking was implemented.

Virgo glitch rate contains peaks largely correlated to unstable weather conditions.

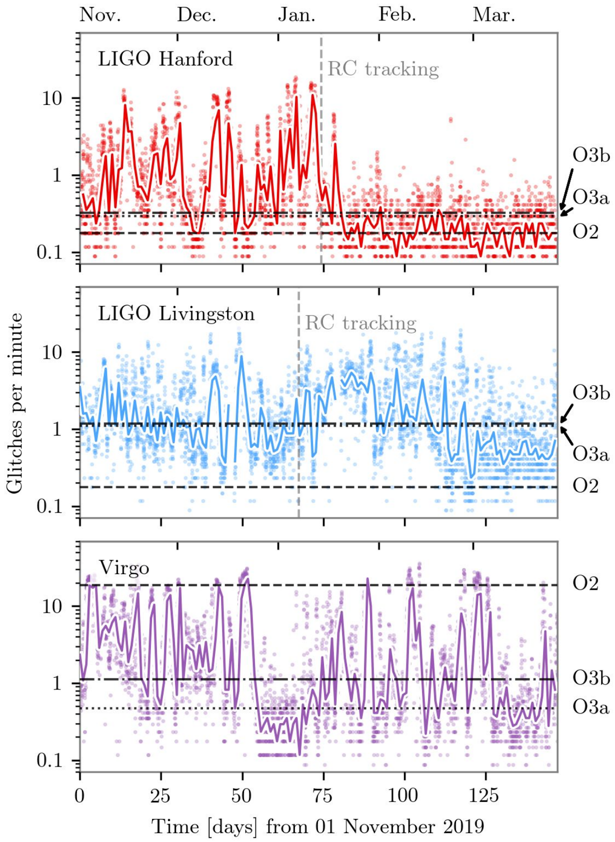

Glitch rate

Scattered light (of various forms) was a major driver of glitch rate at all three detectors

Scattered light tends to be driven by local **ground motion**, and correlated with **bad weather**

For more on O3 scattered light:
Soni *et al.* (2021)
Class. Quant. Grav. 38, 025016

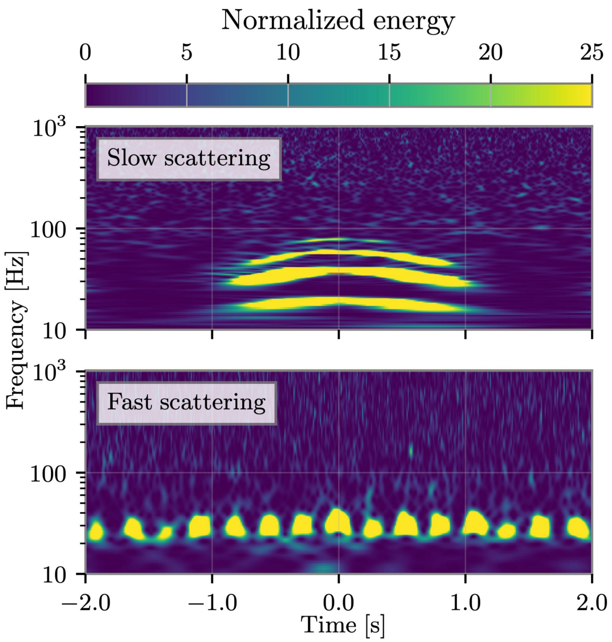

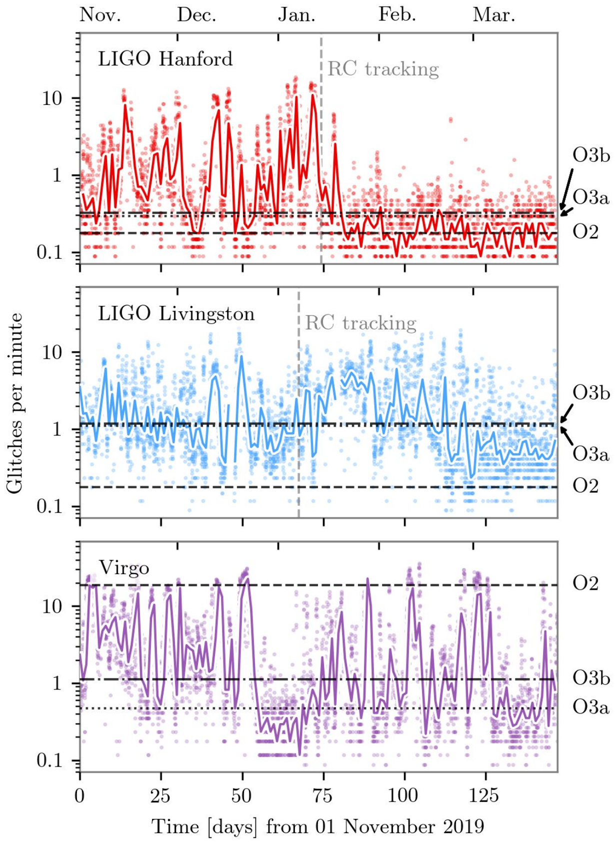

Event validation

Same **event validation** procedures used as in O3a

Candidates in the main event list have a probability of astrophysical origin > 0.5

Noise mitigation includes subtraction of excess noise and glitches

Glitches were modeled with the BayesWave algorithm

No candidates in the main event list were found to be likely instrumental artifacts by event validation procedures.

3 marginal candidates were found to be **likely instrument artifacts.**

Glitch subtraction applied to 8 events before source property analysis.

GW200115_042309

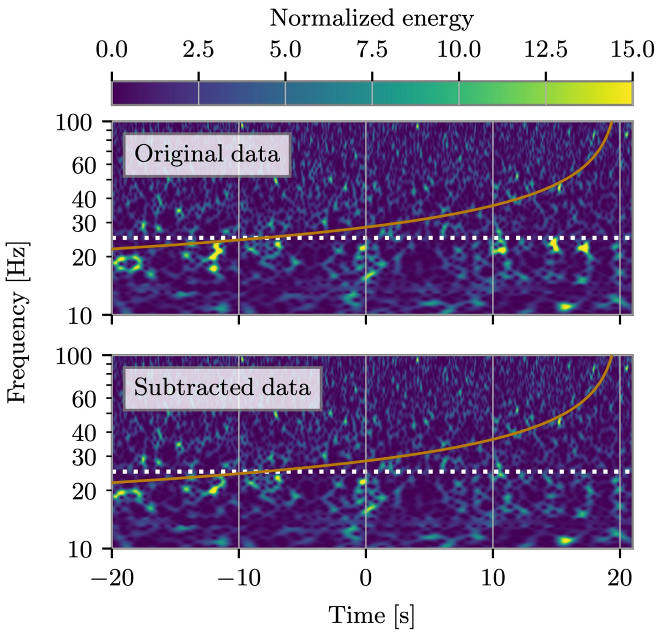

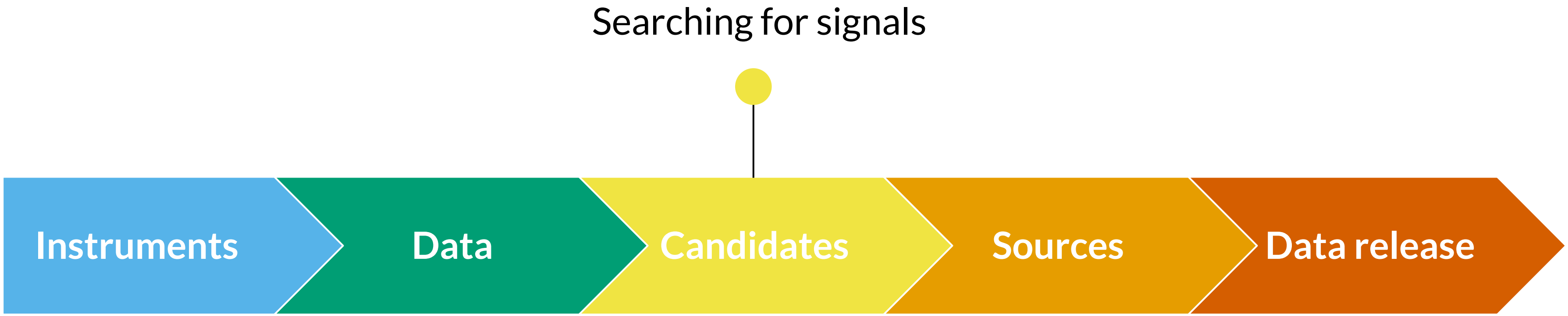

Searching for signals
Instruments
Data
Candidates
Sources
Data release

Detections across observing runs

The event rate in O3b is consistent with O3a and our expectations

Adding 35 new gravitational wave candidates brings our total to 90

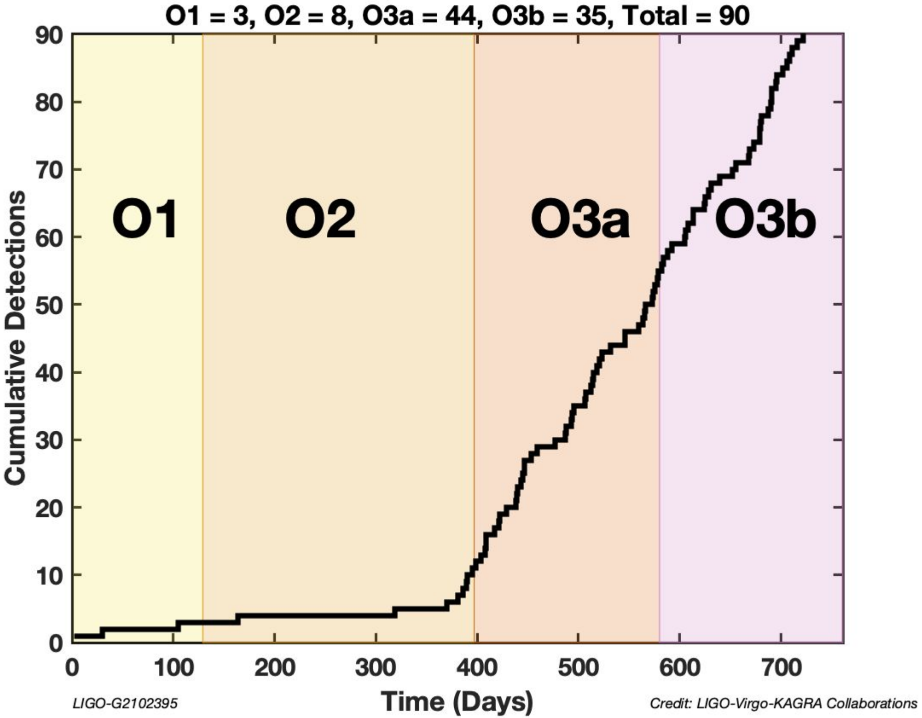

Search methods

Same methods as GWTC-2.1 (GstLAL, MBTA, PyCBC) and GWTC-2 (cWB)

Searches are done on two timescales: low-latency and **offline re-analysis**

Modeled searches

- GstLAL, MBTA, PyCBC Broad, PyCBC BBH
- Assume the source is a compact binary coalescence (CBC)
- Uses matched filtering and banks of template waveforms with varying parameters to find signals in the data
- HL, HV, LV, HLV coincidences
- GstLAL allows for single-detector candidates

Minimally modeled search

- cWB
- Can potentially identify non-CBC sources
- Does **not** use matched filtering or waveforms
- Identifies excess power in coincident strain data to find signals
- HL, HV, LV coincidences

Estimating significance

Follow GWTC-1, GWTC-2.1 in using **p-astro > 0.5** threshold for inclusion in main event list (assuming CBC sources).

Follow GWTC-2.1 in using **FAR < 2 per year** threshold for inclusion in marginal event list.

False alarm rate (FAR)

- How often do we expect noise to produce a trigger with the same ranking statistic?
- Does not take into account any astrophysical information

Probability of astrophysical origin (p-astro)

- Assess significance by comparing the foreground and background ranking statistic distributions, informed by the estimated astrophysical rates
- $$p_{\text{astro}} = p_{\text{BNS}} + p_{\text{NSBH}} + p_{\text{BBH}} = 1 - p_{\text{terr}}$$

Candidate list

Same methods as GWTC-2.1 (GstLAL, MBTA, PyCBC) and GWTC-2 (cWB)

Main event lists: p-astro > 0.5 in at least one pipeline (for CBC sources)

Thresholds for inclusion

- Main event list (35 events)
  - p-astro > 0.5
  - ~10–15% contamination
- Marginal event list (7 events)
  - p-astro < 0.5 but FAR < 2 per year
- Deep sub-threshold list (1041 events)
  - FAR < 2 per day
  - ~2% purity

Low latency vs offline

- 39 events found in low latency
  - 16 retracted
  - 5 events not found offline
- 17 events found offline, not found in low-latency
- 35 events added to the catalog

Candidate list

35 events with
p-astro > 0.5

3 NSBH (or potential NSBH) + GW200105

3 marginal candidates with identified instrumental origin (including cWB only event 200214)

2 single detector candidates + GW200105

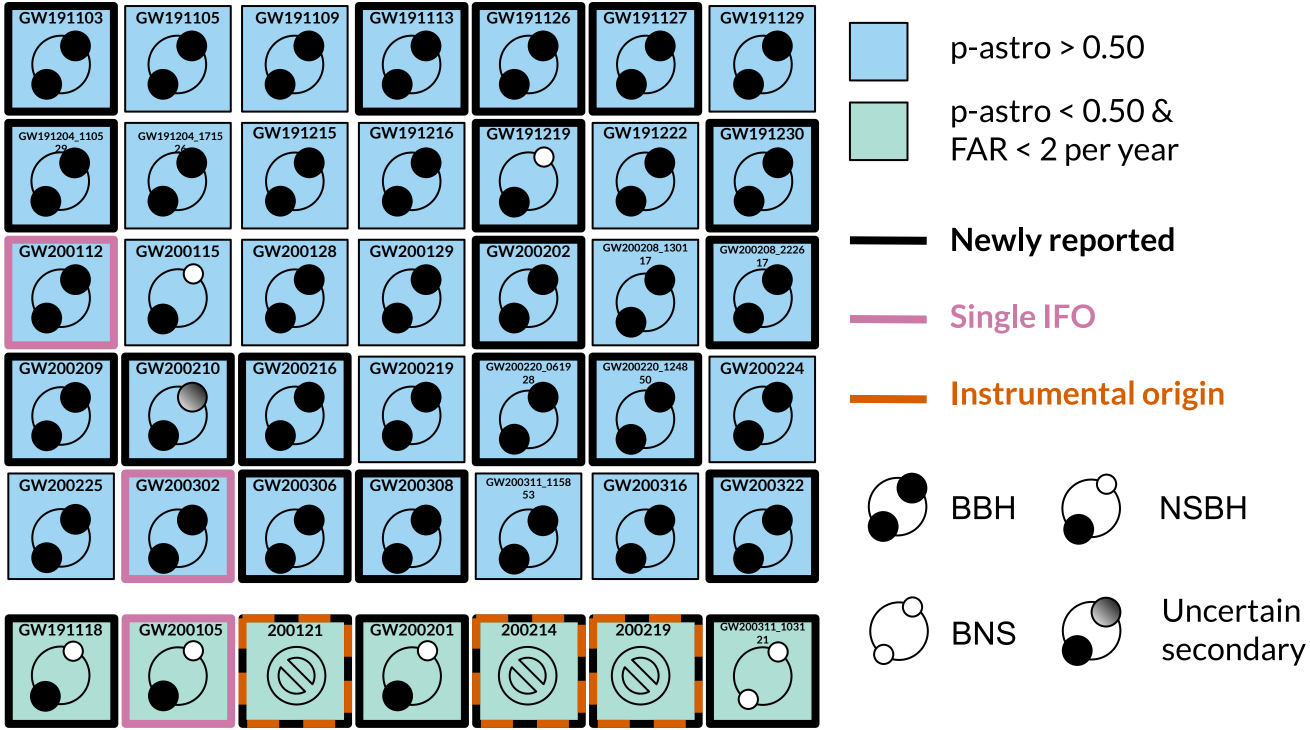

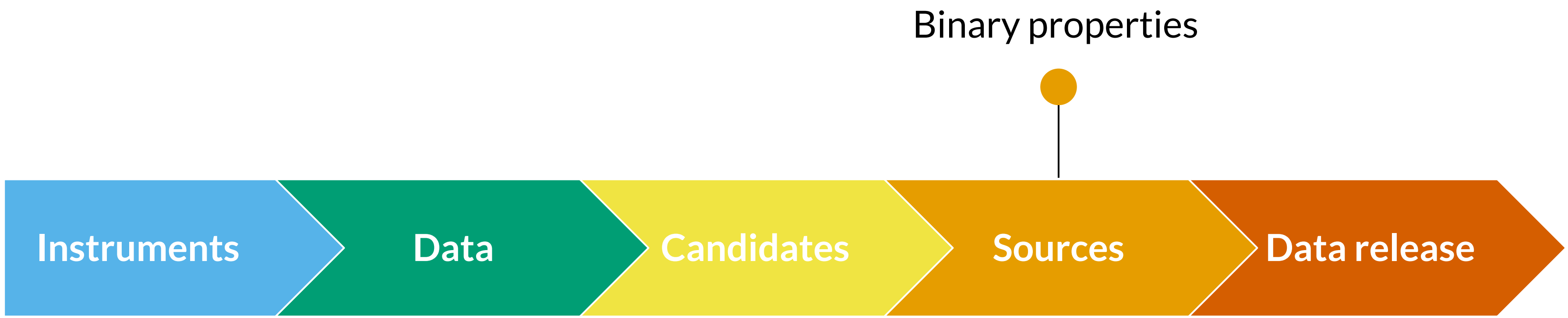
Binary properties
Instruments
Data
Candidates
Sources
Data release

Growing catalogue

GWTC-3 adds **35** events with more than 50% probability of an **astrophysical** source

Total number of candidates is 90

Most are binary black holes **(BBHs)**

Some are neutron star–black hole binaries **(NSBHs)**

Two are binary neutron stars **(BNSs)**

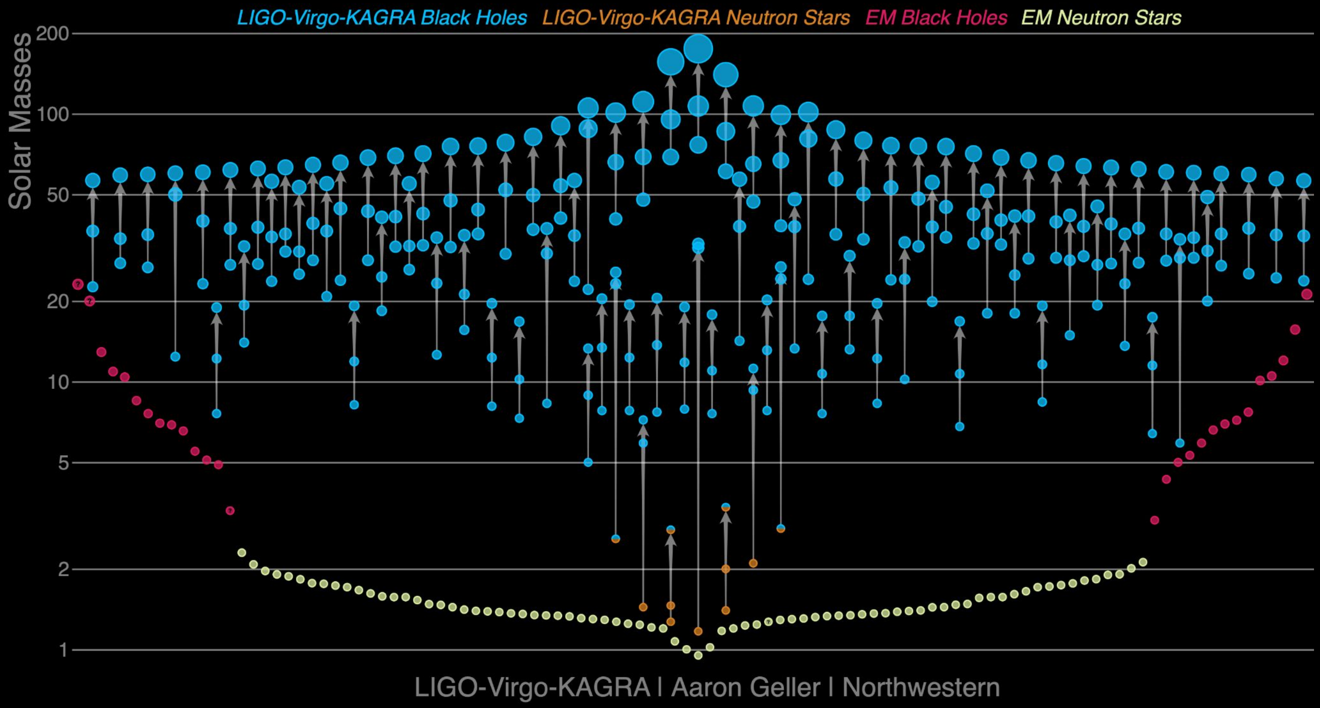

Sources

All signals so far have come from the merger of two compact objects: **neutron stars** and **black holes**

We analyse data to **infer source properties** like masses, spins, distance and sky location

We use the same **waveform models** as GWTC-2.1

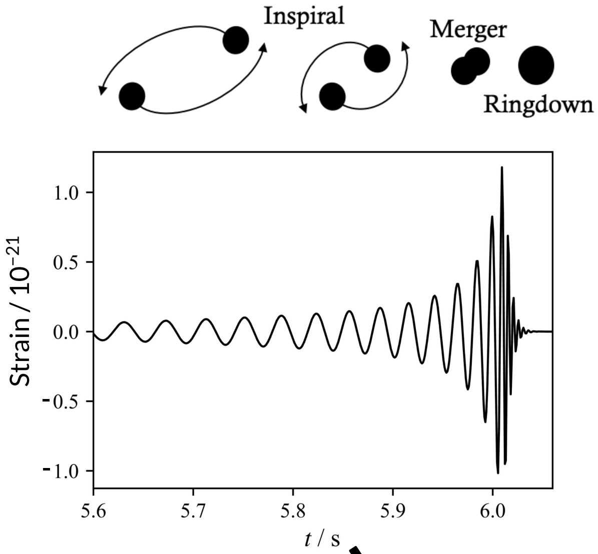

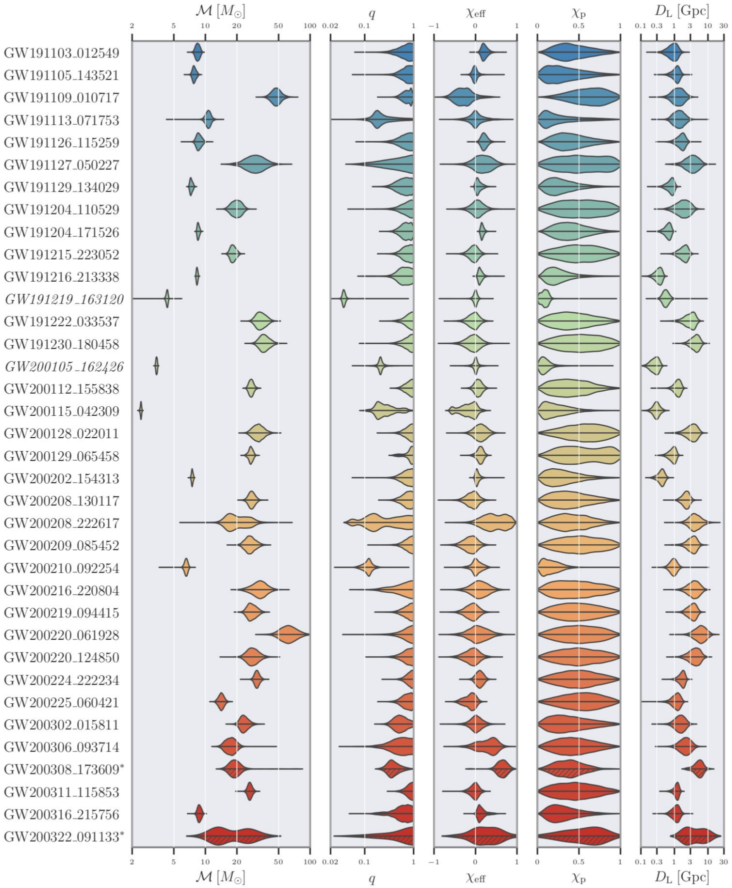

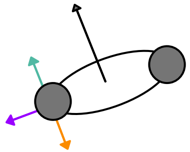

Highlighted events

- **negative** effective inspiral spin, **2nd most massive** in O3b
- least massive BBH in O3b
- **positive** effective inspiral spin
- NSBH, most extreme mass ratio
- NSBH
- **misaligned** spin
- NSBH?
- **most massive** in O3b
- **negative** effective inspiral spin

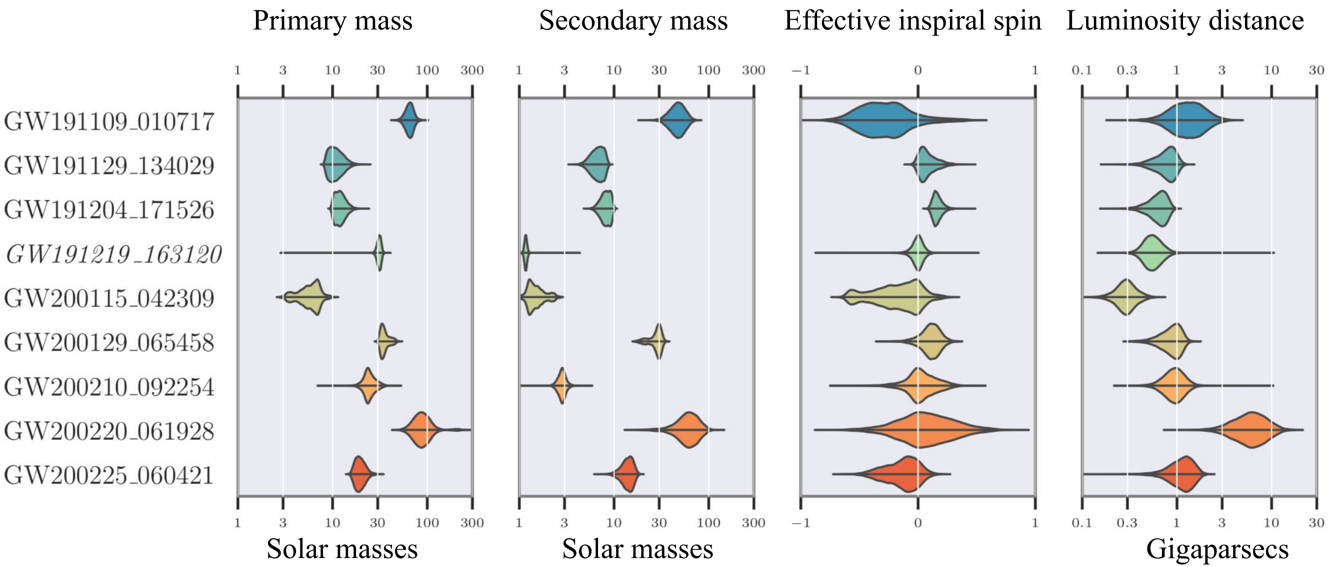

NSBH masses

Mass ratio q is **ratio** of **secondary** to **primary** mass:

$$q = \frac{m_2}{m_1}$$

Coloured contours in this plot are **confident** neutron star–black hole pairs

Grey contours in this plot are **ambiguous**, with secondary that may be a black hole or a neutron star

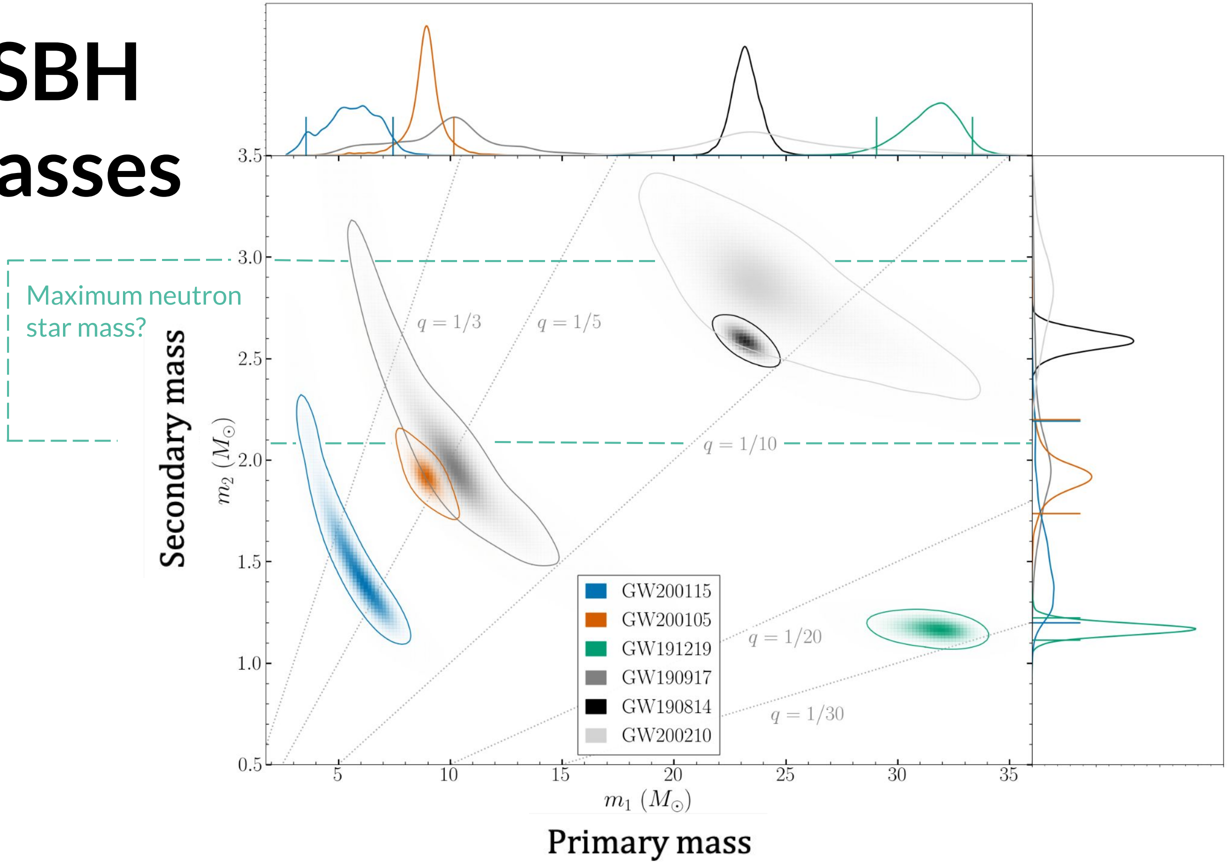

Masses & spins

$$\mathcal{M} = \frac{(m_1 m_2)^{3/5}}{(m_1 + m_2)^{1/5}} \quad \chi_{\rm eff} = \frac{(m_1 \vec{\chi}_1 + m_2 \vec{\chi}_2) \cdot \vec{L}_{\rm N}}{(m_1 + m_2)}$$

Most effective inspiral spins **consistent with zero**

Some events with significant support for negative effective inspiral spins

More events have significant support for positive effective inspiral spins

Consistent with GWTC-2.1

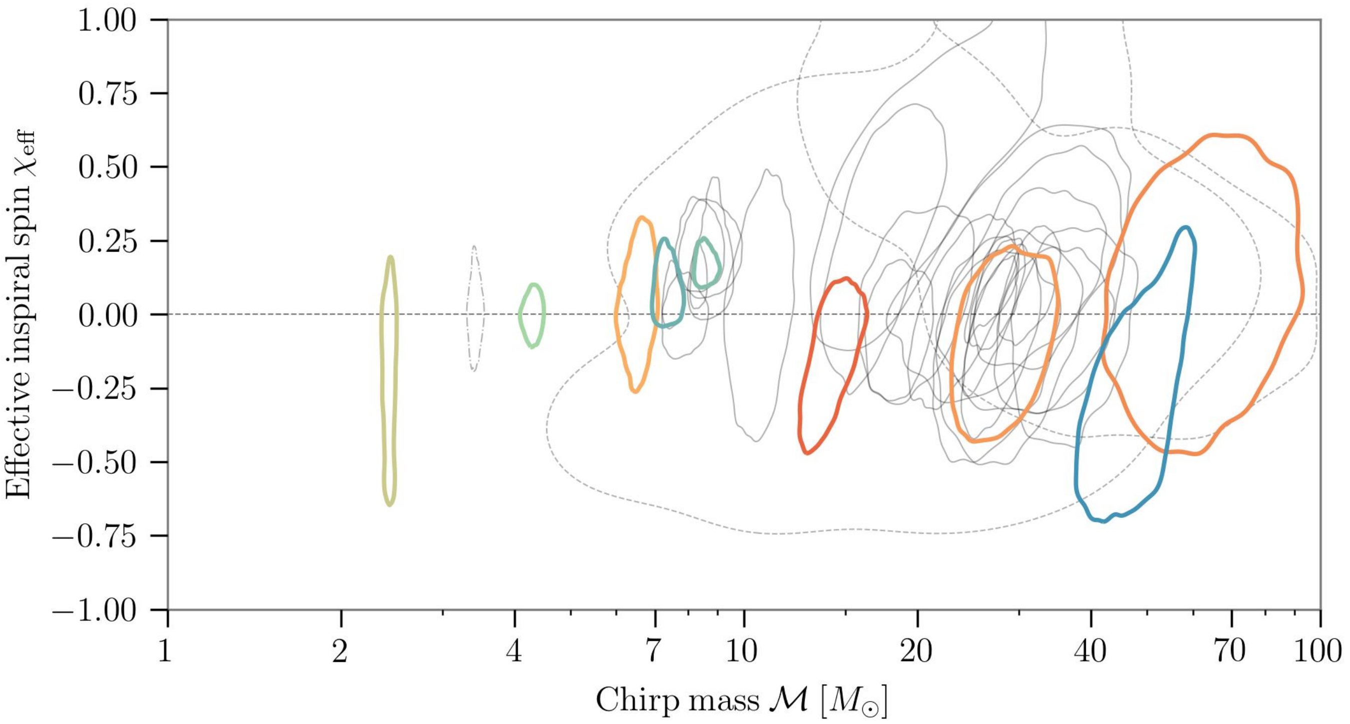

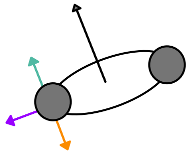

NSBH spins

Primary spin better measured as more important for dynamics

Spin components in the orbital plane better measured for more extreme mass ratios

Spins **approximately aligned** with orbital angular momentum expected for binaries formed in isolation

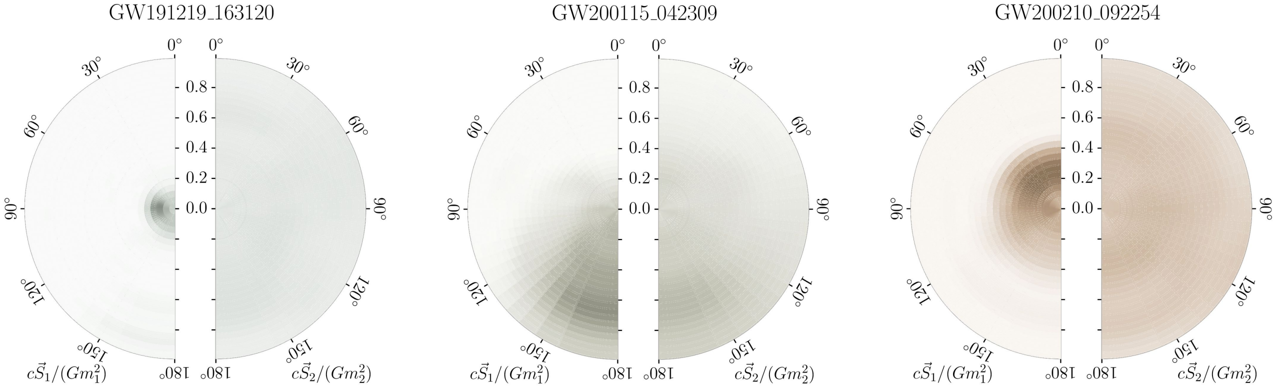

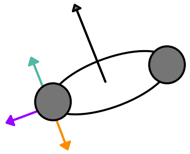

BBH spins: small and positive

Spins expected to be small if angular moment transfer is efficient in stars

Spins in X-ray binaries extend close to the Kerr limit of 1

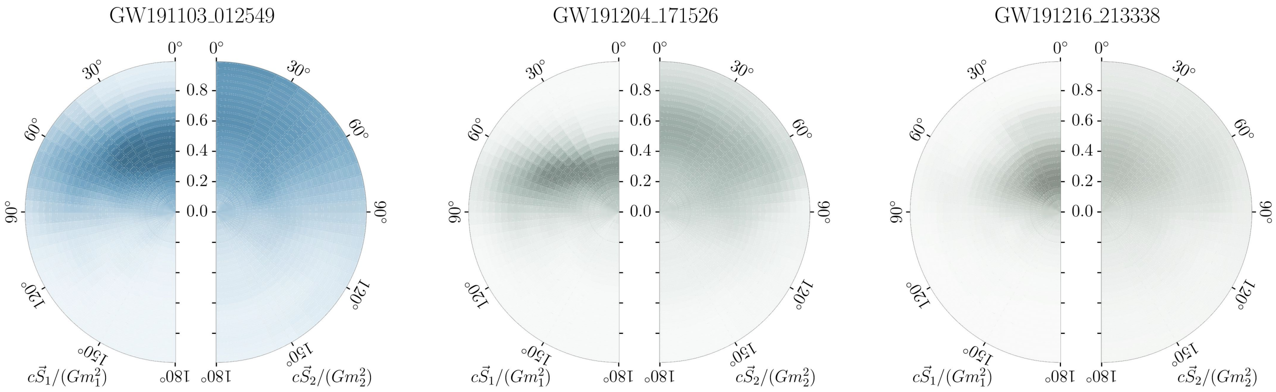

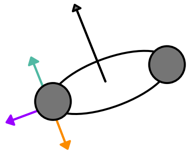

BBH spins: misaligned or negative

Misaligned spins expected for binaries formed dynamically

Equal-mass mergers produce spins around 0.7

GW200129 shows best evidence for **misaligned spins**

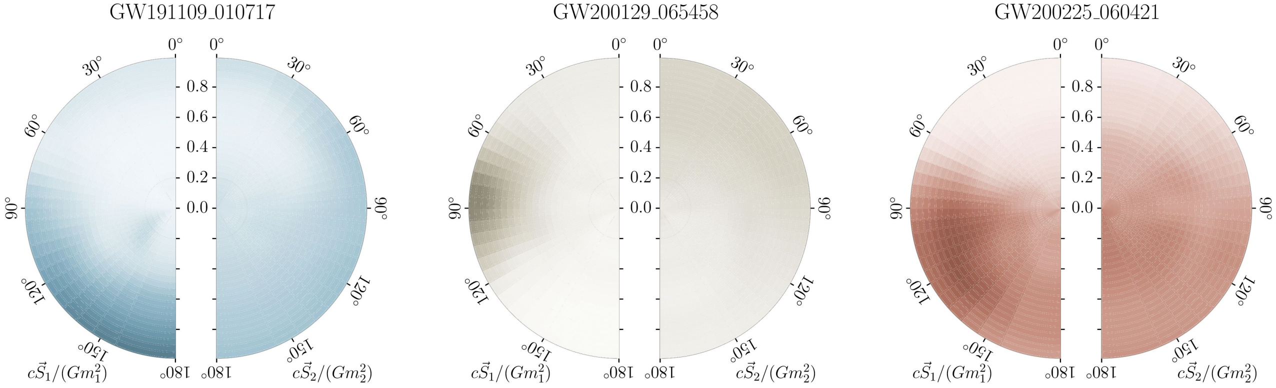

Locations

Localisation strongly depends on number of detectors observing a signal

Smallest 90% credible **sky area** is GW200208_130117 with **30 deg^2** (compare to Moon's area of 0.2 deg^2!)

Smallest 90% credible **sky volume** localised is GW200202 with **0.0024 Gpc^3**

GW200208_130117

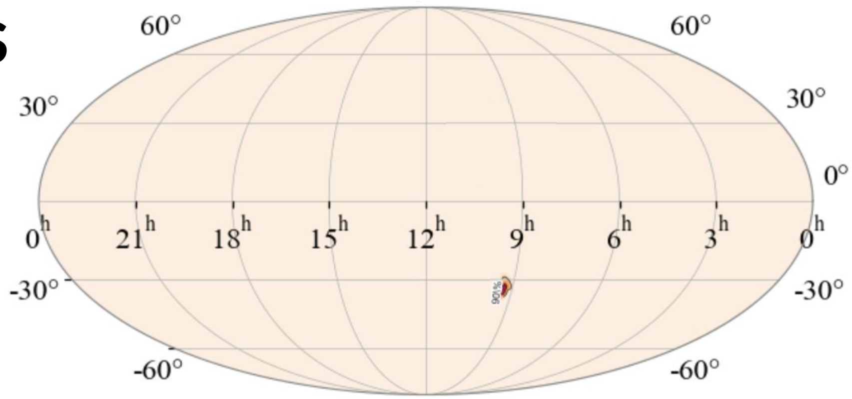

GW200202_154313

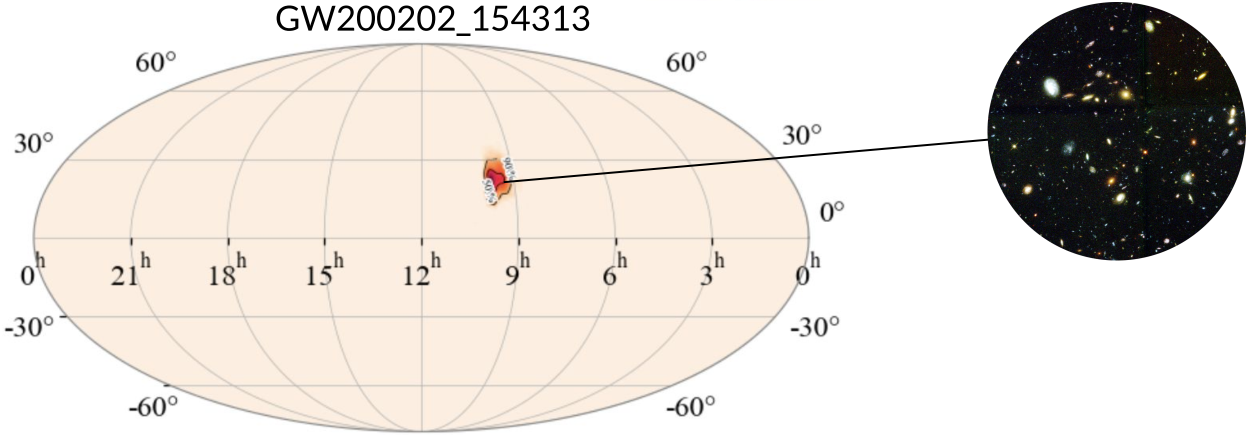


Results & tutorials
Instruments
Data
Candidates
Sources
Data release

Data

Data products mirror the release for GWTC-2.1

Notebooks and example **scripts** included with data products

Gravitational Wave Open Data Workshops provide more resources to understand data analysis

Strain data

Bulk data release available from www.gw-openscience.org/O3/O3b/

Data products

Analysis results available from www.gw-openscience.org/GWTC-3/

- Data-quality files
- Glitch-subtracted data
- Candidate list
- Search sensitivity (O3, and O1+O2+O3)
- Parameter-estimation results
- Data behind the figures

Summary

A total of **90** candidates with p-astro > 0.5 plus many more lower probability candidates

Applications to **cosmology** (9 Dec), **astrophysics** (10 Dec) and **tests of general relativity** (20 Jan)

O4 target BNS ranges
LIGO: 160–190 Mpc
Virgo: 80–115 Mpc
KAGRA: >1 Mpc

O3 saw the detector network reach its greatest performance to date

35 O3b candidates with p-astro > 0.5

O3b candidates have a diverse range of masses and spins, and include confident neutron star–black holes

O4 scheduled to start in mid-December 2022 with LIGO, Virgo and KAGRA

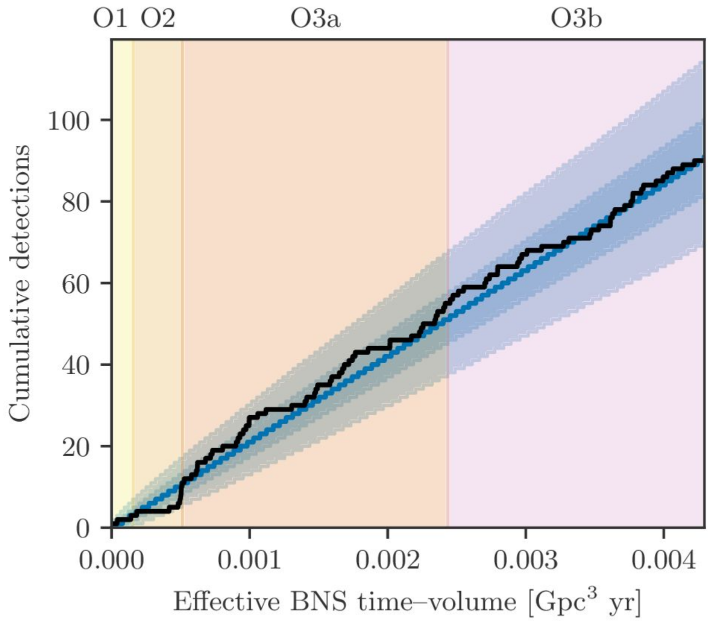

This material is based upon work supported by NSF’s LIGO Laboratory which is a major facility fully funded by the National Science Foundation. The authors also gratefully acknowledge the support of the Science and Technology Facilities Council (STFC) of the United Kingdom, the Max-Planck-Society (MPS), and the State of Niedersachsen/Germany for support of the construction of Advanced LIGO and construction and operation of the GEO 600 detector. Additional support for Advanced LIGO was provided by the Australian Research Council. The authors gratefully acknowledge the Italian Istituto Nazionale di Fisica Nucleare (INFN), the French Centre National de la Recherche Scientifique (CNRS) and the Netherlands Organization for Scientific Research, for the construction and operation of the Virgo detector and the creation and support of the EGO consortium. The authors also gratefully acknowledge research support from these agencies as well as by the Council of Scientific and Industrial Research of India, the Department of Science and Technology, India, the Science & Engineering Research Board (SERB), India, the Ministry of Human Resource Development, India, the Spanish Agencia Estatal de Investigación, the Vicepresidència i Conselleria d'Innovació, Recerca i Turisme and the Conselleria d'Educació i Universitat del Govern de les Illes Balears, the Conselleria d'Innovació, Universitats, Ciència i Societat Digital de la Generalitat Valenciana and the CERCA Programme Generalitat de Catalunya, Spain, the National Science Centre of Poland and the Foundation for Polish Science (FNP), the Swiss National Science Foundation (SNSF), the Russian Foundation for Basic Research, the Russian Science Foundation, the European Commission, the European Regional Development Funds (ERDF), the Royal Society, the Scottish Funding Council, the Scottish Universities Physics Alliance, the Hungarian Scientific Research Fund (OTKA), the French Lyon Institute of Origins (LIO), the Belgian Fonds de la Recherche Scientifique (FRS-FNRS), Actions de Recherche Concertées (ARC) and Fonds Wetenschappelijk Onderzoek – Vlaanderen (FWO), Belgium, the Paris Île-de-France Region, the National Research, Development and Innovation Office Hungary (NKFIH), the National Research Foundation of Korea, the Natural Science and Engineering Research Council Canada, Canadian Foundation for Innovation (CFI), the Brazilian Ministry of Science, Technology, and Innovations, the International Center for Theoretical Physics South American Institute for Fundamental Research (ICTP-SAIFR), the Research Grants Council of Hong Kong, the National Natural Science Foundation of China (NSFC), the Leverhulme Trust, the Research Corporation, the Ministry of Science and Technology (MOST), Taiwan, the United States Department of Energy, and the Kavli Foundation. The authors gratefully acknowledge the support of the NSF, STFC, INFN and CNRS for provision of computational resources. Computing was performed on the OzSTAR Australian national facility at Swinburne University of Technology, which receives funding in part from the Astronomy National Collaborative Research Infrastructure Strategy (NCRIS) allocation provided by the Australian Government. We thankfully acknowledge the computer resources at MareNostrum and the technical support provided by Barcelona Supercomputing Center (RES-AECT-2021-2-0021). This work was supported by MEXT, JSPS Leading-edge Research Infrastructure Program, JSPS Grant-in- Aid for Specially Promoted Research 26000005, JSPS Grant-in-Aid for Scientific Research on Innovative Areas 2905: JP17H06358, JP17H06361 and JP17H06364, JSPS Core-to-Core Program A. Advanced Research Networks, JSPS Grant-in-Aid for Scientific Research (S) 17H06133, the joint research program of the Institute for Cosmic Ray Research, University of Tokyo, National Research Foundation (NRF) and Computing Infrastructure Project of KISTI-GSDC in Korea, Academia Sinica (AS), AS Grid Center (ASGC) and the Ministry of Science and Technology (MoST) in Taiwan under grants including AS-CDA-105-M06, Advanced Technology Center (ATC) of NAOJ, and Mechanical Engineering Center of KEK.

We would like to thank all of the essential workers who put their health at risk during the COVID-19 pandemic, without whom we would not have been able to complete this work.

Questions

Waveform reconstructions

Analysis closely mirrors GWTC-2

Unmodeled reconstructions identify potential inconsistencies in the source properties reconstruction

- Minimal assumptions on signal shape:
  - cWB: constrained maximum-likelihood reconstruction
  - BayesWave: median of the time-domain waveform

- On-source: reconstructed waveform of candidate
- Off-source: injections of waveform in the background around candidate times
- Match parameter as a measure of waveform consistency:

$$\mathcal{O}(h_1,\, h_2) = \frac{\langle h_1 \mid h_2 \rangle}{\sqrt{\langle h_1 \mid h_1 \rangle \langle h_1 \mid h_2 \rangle}}$$

Waveform reconstructions

The match–match plot displays possible inconsistencies between the on-source reconstruction and off-source distribution

Different accuracies due to different number of off-source injections

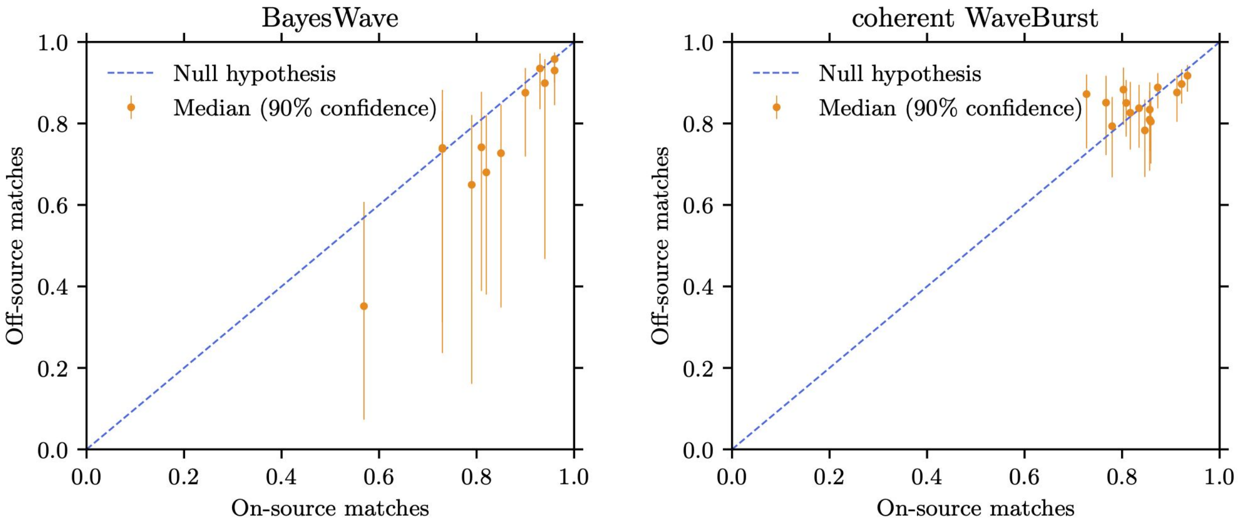

No inconsistency between minimally-modeled waveform reconstruction and parameter-estimation results

Waveform reconstructions

The p-value plot shows any candidate that significantly deviates from the expected statistical distribution

Different accuracies due to different number of off-source injections

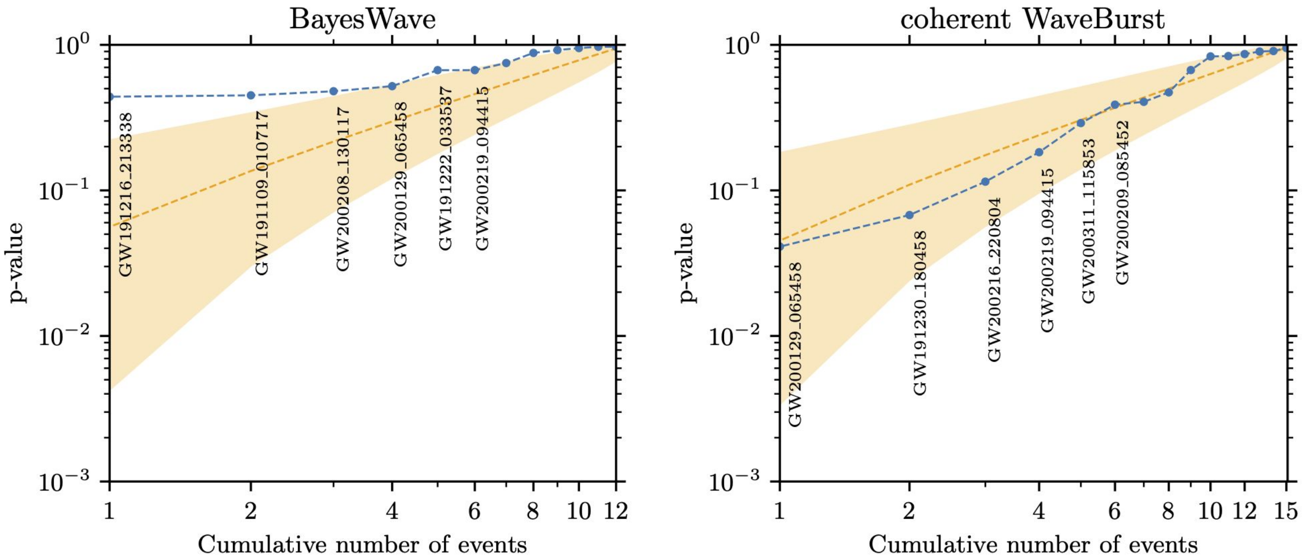

No outlier events are detected by the p-value plot (larger deviation in the BayesWave plot is not statistically significant)

Template bank parameters

Model signals as **compact binary coalescence** (**CBC**)

Waveforms depend on intrinsic source parameters: component masses and the dimensionless component spins

Spins are allowed to be anti-aligned or aligned

$$\mathcal{M} = \frac{(m_1 m_2)^{3/5}}{(m_1 + m_2)^{1/5}}$$

$$q = \frac{m_2}{m_1}$$

$$\chi_{\rm eff} = \frac{(m_1\vec{\chi}_1 + m_2\vec{\chi}_2)\cdot \vec{L}_{\rm N}}{(m_1+m_2)}$$

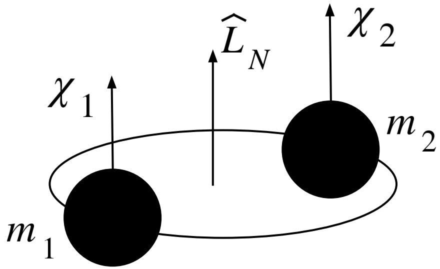

Template bank total masses

- **MBTA:** 2–100 $M_\odot$ for m_2 < 2 $M_\odot$, 2–200 $M_\odot$ otherwise
- **GstLAL:** 2–758 $M_\odot$
- **PyCBC-Broad:** 2–500 $M_\odot$
- **PyCBC-BBH:** 10–500 $M_\odot$

Mass ratio

- **MBTA:** no mass ratio restraints
- **GstLAL:** 0.02–1 (depending on parameter space region)
- **PyCBC-Broad:** 0.01–1
- **PyCBC-BBH:** ⅓–1

Maximum component spin magnitudes

- **MBTA:** 0.05 for m_i < 2 $M_\odot$, 0.997 otherwise
- **GstLAL:** 0.05 for m_i < 3 $M_\odot$, 0.999 otherwise
- **PyCBC-Broad:** 0.05 for m_i < 2 $M_\odot$, 0.998 otherwise
- **PyCBC-BBH:** 0.998

Minimally modeled search

When accurate models of sources are unavailable and templates cannot be calculated

When waveforms have unexpected properties or are stochastic

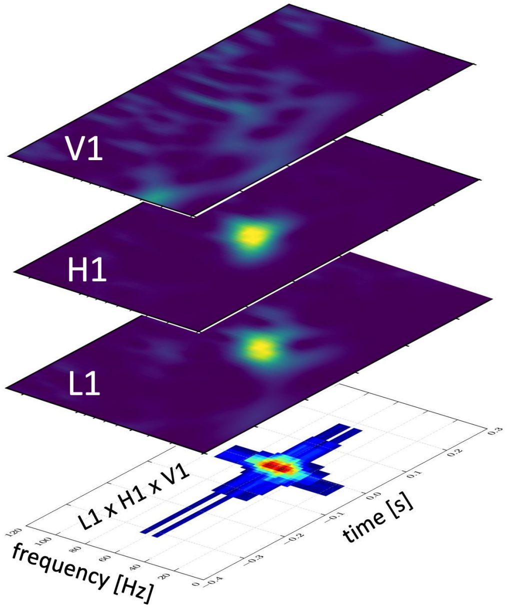

Examples of astrophysical sources

- Binaries: regular CBCs, binaries with eccentric orbits, intermediate-mass black holes
- Stochastic: core-collapse supernovae, neutron star glitches
- Unexpected or unknown

Method

- Complements the modeled searches
- Time-frequency decomposition using wavelets
- Coincident excess power in detectors' strain data

Probability of astrophysical origin

p-astro
Probability that the source belongs to an astrophysical population of compact binaries

Class membership is based on component masses only

GstLAL & PyCBC: Neutron star/black hole boundary at 3 solar masses
MBTA: Neutron star/black hole mass gap at 2.5–5 solar masses
cWB: No mass division

Each pipeline computes p-astro using foreground (signal) $f(x)$ and background (noise) $b(x)$ distributions of the ranking statistic x:

- Assumptions of population models for the foreground
- Estimation of the background directly from the data
- The astrophysical and background rates are inferred from the data through counts Λ_f, Λ_b

Astrophysical source classification is performed by computing membership probabilities:

- Three astrophysical classes considered {BNS, NSBH, BBH}:

$$p_\alpha = \frac{\Lambda_\alpha f_\alpha(x)}{\Lambda_b b(x) + \sum_{\beta \in \{\text{BNS, NSBH, BBH}\}} \Lambda_\beta f_\beta(x)} \qquad p_{\text{astro}} = p_{\text{BNS}} + p_{\text{NSBH}} + p_{\text{BBH}}$$

GW191219_163120

Found only by PyCBC Broad analysis

Search properties
FAR = 4.0 per year
SNR = 8.9
p-astro = 0.82

Inferred properties
Mass ratio < 0.041
Primary mass ~ 31 solar mass
Secondary mass ~ 1.2 solar mass

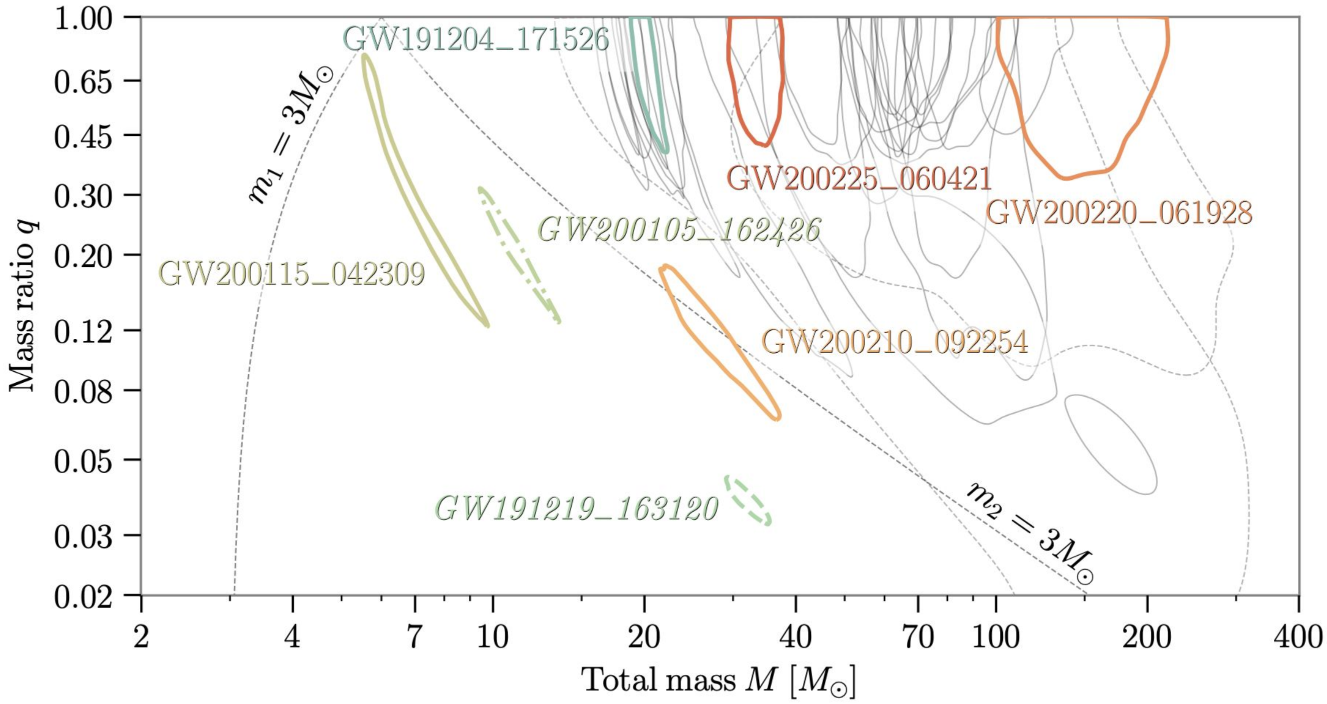

GW200105_162426

GW200105 is a GstLAL **single-detector** candidate

GW200105 clearly stands out from the background

p-astro = 0.36
GWTC-3 FAR = 0.2 per year
Initial discovery paper FAR = 0.36 per year

For more:
LVK (2021)
Astrophys. J. Lett. 915, L5

Single-detector significance limited by observing time: need to extrapolate background

Cannot use coincidence between detectors

p-astro is informed by **astrophysical event rates**: uncertain when we have small number of sources, can be re-evaluated in the future

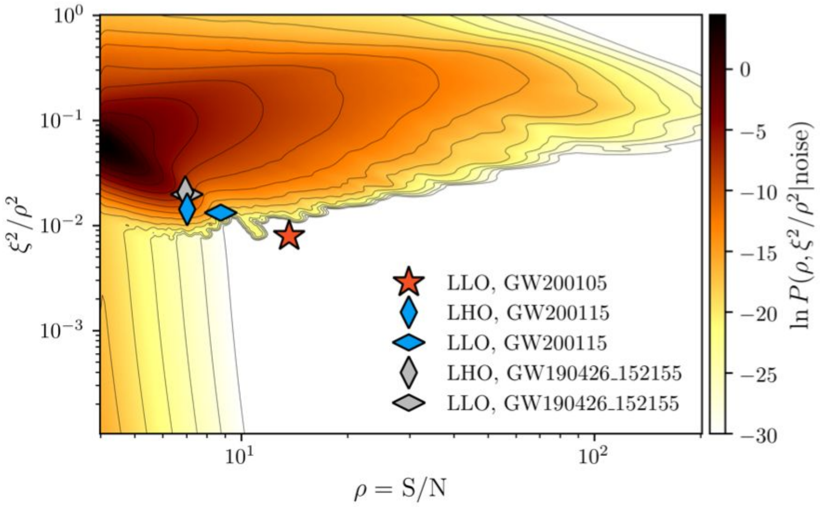

cWB-only candidates

3 candidates were identified **only** by cWB

p-astro > 0.5 **assuming** a CBC source, but we do not have any counterpart from matched-filter search pipelines to corroborate the source assumption

FAR < 2.0 per year

All show signs of **instrumental origin**

Single-interferometer **glitching activity** close to the events. Glitches are incoherent, but can still affect detection

Coherent energy time–frequency morphology reconstructed by cWB does not match observations of CBCs

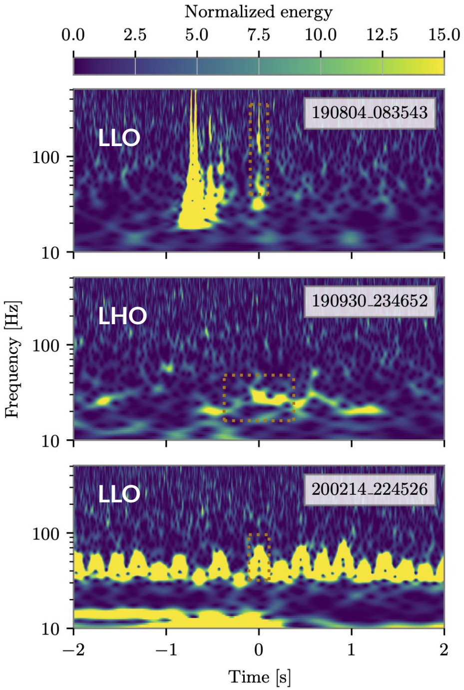

Time–frequency spectrograms of data

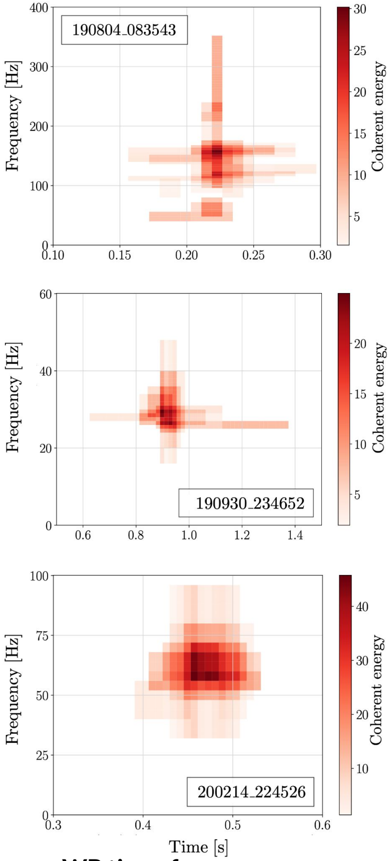

cWB time–frequency maps

Search sensitivity

Search sensitivity quantified by search **volume–time (VT)**

VT calculated at 12 points in mass space for injections found with p-astro > 0.5

Mass combinations cover **binary black holes**, **neutron star–black holes** and **binary neutron stars**

Different pipelines comparatively more sensitive at different points, as expected

VT for injections found by **any pipeline** with p-astro > 0.5 most closely matches GWTC-3 search

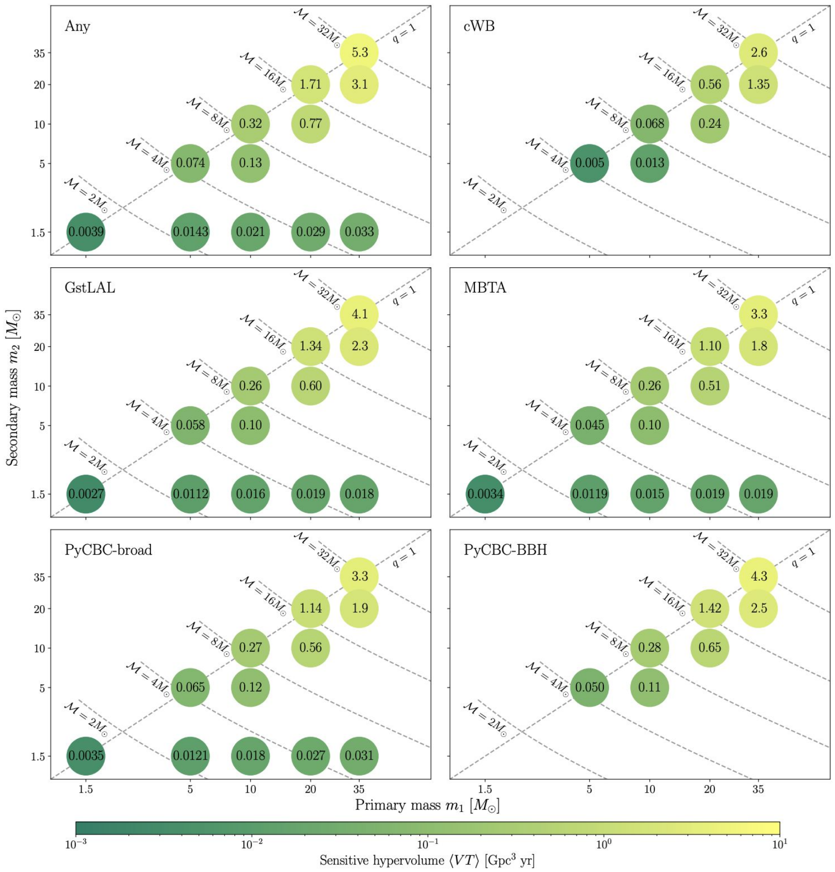

Reaction chain

Light scattering is a common source of transient noise

Slow scattering is caused by light reflected from the electrostatic drive (ESD) on the reaction mass

Reaction-chain tracking minimises relative motion between reaction mass and test mass thereby reducing the slow scattering glitch rate

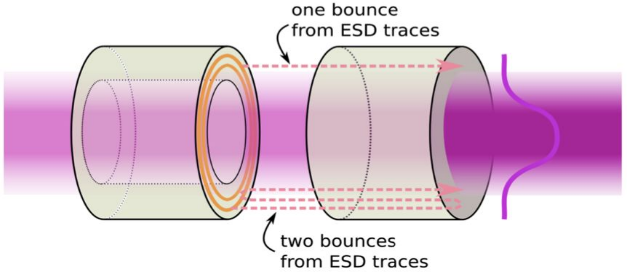

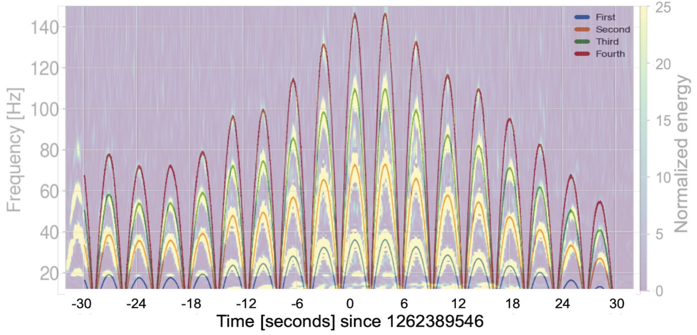

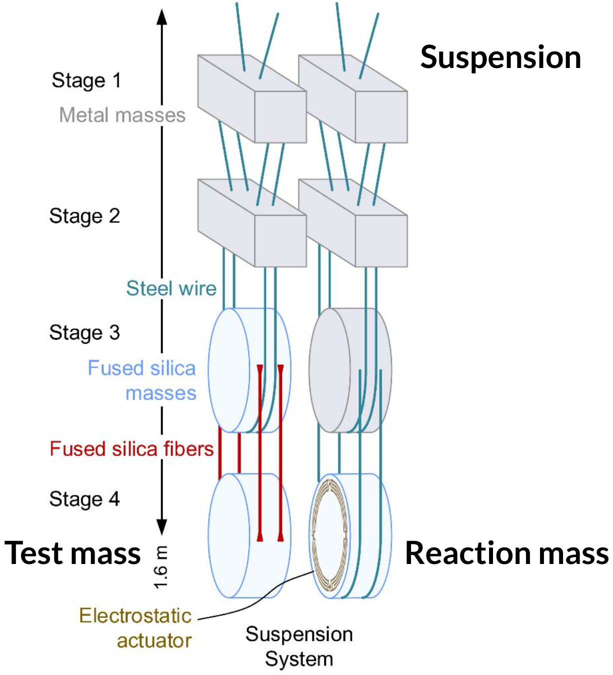

Slow scattering

Light scattering glitches were common in LIGO Livingston and LIGO Hanford

Presence linked to **ground motion**

For more:
Soni *et al.* (2021) Class. Quant. Grav. 38, 025016